Triaxe archeointensity analysis

Yves Gallet, Maxime Le Goff, Agnès Genevey

Triaxe archeointensity analysis

Yves Gallet [a], Maxime Le Goff [a], Agnès Genevey [b]

[a] Université Paris Cité, Institut de Physique du Globe de Paris, CNRS, 1 rue Jussieu, F-75005 Paris, France

[b] Sorbonne Université, CNRS, Laboratoire d'Archéologie Moléculaire et Structurale, 4 place Jussieu, F-75005 Paris, France

Abstract

Since 2004, numerous archeomagnetic intensity data have been obtained using the vibrating sample magnetometer Triaxe, which measures full-vector magnetization directly at high temperatures, in either an applied or zero field. Satisfactory comparisons have been made between Triaxe intensity data and results derived from more conventional Thellier-Thellier type techniques, indicating the reliability of Triaxe data. For each specimen analyzed, a Triaxe archeointensity value is obtained from the average of R'(Ti) data. The R'(Ti) parameter is determined every 5°C and corresponds to the ratio, multiplied by the laboratory field intensity, between the natural remanent magnetization (NRM) and laboratory-thermoremanent magnetization (TRM_{lab}) fractions that are lost between reference temperature T1 and a given temperature Ti between T1 and reference temperature T2. Here, we introduce an additional parameter, based on so-called AutoR'(Ti) data, to facilitate and improve the interpretation of Triaxe measurements. Each individual AutoR'(Ti) datum corresponds to an averaged R'(Ti) value; the AutoR'(Ti) dataset is then obtained by gradually decreasing the temperature range from T1 to T2 to a minimum temperature interval near T2. Several examples of Triaxe measurements show the value of using AutoR'(Ti) data to isolate the most appropriate temperature range for an intensity determination, as well as to characterize the cooling rate effect on TRM acquisition. In particular, these experiments confirm that the Triaxe procedure minimizes this effect because, when it is present, it appears to be largely due

to magnetic grains with high unblocking temperatures (>~350°C). Moreover, the AutoR'(Ti) dataset provides alternatives for estimating mean archeointensity values at both the fragment and fragment-group levels. We show that the simple approach used so far, based on the average of the R'(Ti) data determined over a single temperature interval, provides results as reliable as those derived from other options.

Keywords: Archeomagnetic intensity data, experimental protocol, Triaxe magnetometer, cooling rate effect

1. Introduction

Archeomagnetism, based on the analysis of the magnetic properties of baked-clay archeological artifacts, is a unique tool for tracing the evolution of the Earth's magnetic field over the past ten millennia. In general, the strength of this discipline lies in the precision of the dating of the material studied and that of the experimental determinations. However, the reliability and accuracy of archeomagnetic intensity data have been subject to numerous evaluations based on selection criteria that vary from one study to another (Genevey et al., 2008; Paterson et al., 2014; Hervé et al., 2019a; Brown et al., 2021). It appears that archeointensity data are often of uneven quality; biased (e.g., due to no or insufficient correction for the cooling rate effect on thermoremanent magnetization acquisition) or erroneous (e.g., due to undetected heating-induced magnetomineralogical alteration) values are likely present in the data compilations (e.g. Licht et al., 2013). Although a set of selection criteria is clearly useful, it remains very difficult to identify all inaccurate values, with the intent to eliminate them or at least reduce their detrimental effect on the development of archeo-geomagnetic field models (Constable et al., 2016; Hellio and Gillet, 2018; Campuzano et al., 2019; Pavón-Carrasco et al., 2021).

For nearly 20 years, our research group has been conducting archeointensity studies in different regions of the world, with a focus on Western Europe and the Near East (Genevey et al., 2013; 2016; 2021; Gallet et al., 2014; 2015; 2020). In recent years, these studies have utilized the Triaxe magnetometer and an original experimental protocol adapted to this instrument that were developed in our laboratory (Le Goff and Gallet, 2004). Comparative studies featuring other paleo-archeointensity protocols (Thellier and Thellier, 1959; Coe, 1967; Aitken et al., 1988; Yu et al., 2004) have shown the reliability of the intensity measurements obtained using the Triaxe protocol (Genevey et al., 2009; Hartmann et al., 2010; 2011; Hervé et al., 2017; Shaar et al., 2020). Nevertheless, we have remained concerned about the reliability of the Triaxe intensity data and are always striving to strengthen it.

The Triaxe is a vibrating sample magnetometer with a sensitivity of ~10^{-8} Am^2, allowing to quasi-continuously measure the full vector of the remanent magnetization of a small cylindrical specimen (<1 cm^3) directly at high temperatures of up to 650°C, in either a zero field or in a field in any direction, and at a fixed intensity up to 200 μT (Le Goff and Gallet, 2004; Fig. 1). While taking measurements, it demagnetizes the natural remanent magnetization (NRM) of the specimen, which, in the case of ceramic samples, consists of thermoremanent magnetization, as well as acquires (and subsequently demagnetizes) a laboratory thermoremanent magnetization (TRM_{lab}) of the specimen with a direction that is automatically adjusted according to that of the characteristic magnetization carried by that specimen. Further details on the principles of measurements with a vibrating sample magnetometer can be found in Poidras et al. (2009).

The Triaxe archeointensity protocol developed by Le Goff and Gallet (2004) has been applied to thousands of archeological baked-clay specimens of various ages and origins (e.g., pottery, pavement, architectural brick or kiln) from different geographical regions (see above

76 references). Since the original publication, we have developed further our procedure for
77 analyzing Triaxe measurements. Although it has been used routinely for several years, it has
78 not been presented until now. Therefore, the objective of this study is to describe in more
79 detail the additional analyses performed to support and consolidate the interpretation of
80 Triaxe measurements, and revisiting the question of the cooling rate effect on TRM
81 acquisition. For archeointensity data, this effect is arguably difficult to estimate quantitatively
82 (e.g. Fox and Aitken, 1980; Genevey and Gallet, 2002; Genevey et al., 2003; Hervé et al.,
83 2019b; Kostadinova-Avramova and Jordanova, 2019); however, the Triaxe method largely
84 allows it to be taken into account experimentally via a simple and direct approach.

85

86 **2. Description of the Triaxe archeointensity protocol**

87 The Triaxe protocol is derived, albeit with major differences, from a method initially
88 proposed by Boyd (1986) and then apparently never exploited beyond the original
89 publication. It also shares common features with the method developed by Wilson (1961) in
90 that the magnetization measurements are continuously carried out at high temperatures and
91 the NRM is replaced by a laboratory TRM in a single heating step. The constancy of the
92 magnetization ratio as a function of temperature is then used to determine an intensity value
93 (e.g. Lhuillier et al., 2019). The basic philosophy of the Triaxe method is to replace the NRM
94 with the laboratory-TRM (TRM_{lab}) under similar field conditions (direction and intensity).
95 The procedure consists of five series of automatic measurements taken over a period typically
96 lasting just over two hours (~2h-15min). Before starting the measurements, three parameters
97 are set. The first two parameters are the temperatures referred to as T1 and T2. T1 is set low,
98 generally at 150°C, i.e., at a temperature generally sufficient to eliminate most of the possible
99 viscous remanent magnetization component. T2 is usually set at around 500°C, a temperature
100 at which most of the NRM is isolated, but it can be set higher or lower depending on the

thermal demagnetization of the specimen. T1 and T2 determine the range of temperatures over which the intensity analyses will be carried out. The third parameter is the field intensity (H_{lab}) for TRM_{lab} acquisition. This acquisition is routinely performed with a cooling rate of 25°C per minute, but this rate, which is also considered a parameter, can be adjusted (see below). Note that the laboratory field intensity must be set as close as possible to the expected intensity (see discussion in Le Goff and Gallet, 2004).

The five series of measurements, referred to as M1 to M5, are as follows (Fig. 2):

M1: In a zero field, after preliminary heating from room temperature to T1, the magnetization of the sample is measured continuously up to T2. This procedure leads to the demagnetization of the NRM up to T2.

M2, M3: Still in a zero field, the sample is cooled back to T1 (M2) and then reheated to T2 (M3). These two steps whose reversibility attests the thermal stability of the magnetization fraction remaining blocked at T2 allow the thermal variation in the spontaneous magnetization (Js) between T1 and T2 to be characterized (e.g. Dunlop and Özdemir, 1997). The effect of the magnetization fraction blocked at T2 on the magnetic fractions isolated between T1 and T2 is then taken into account by subtracting each M3 value measured at a given temperature from the M1 and M5 values (see below) measured at the same temperature, thus isolating only the fraction of magnetization involved in the archeointensity experiments.

M4: After setting H_{lab}, the magnetization is measured while the sample is cooled to T1. This step leads to the acquisition of TRM_{lab}. The direction of H_{lab} is automatically adjusted so that the TRM_{lab} is closely parallel to the characteristic NRM.

M5: In a zero field, the magnetization is measured while the sample is again heated to T2, demagnetizing the TRM_{lab}.

The procedure ends with a rapid cooling of the sample to room temperature.

125 The derivation of an archeointensity value from the measurements above is explained
126 in detail by Le Goff and Gallet (2004). The method uses M1, M3 and M5, which are acquired
127 with the temperature increasing at a rate of 30°C per minute. The archeointensity value is then
128 estimated from the ratio between the NRM and TRM_{lab} fractions lost between T1 and any
129 temperature Ti between T1 and T2.

130 The intensity value R'(Ti) is obtained at Ti by the formula:

131 $$R'(Ti) = H_{lab} \times \Delta'1(Ti) / \Delta'5(Ti)$$

132 where

133 $$\Delta'1(Ti) = (M1(T1) - M1(Ti)) - (M3(T1) - M3(Ti))$$

134 and

135 $$\Delta'5(Ti) = (M5(T1) - M5(Ti)) - (M3(T1) - M3(Ti)).$$

136 For each specimen, it is therefore possible to determine a mean archeointensity value
137 averaging all R'(Ti) data points obtained between T1 and T2 (after interpolation every 5°C
138 and exclusion of the four first data points, for which the NRM and TRM_{lab} lost fractions are
139 too small to provide a meaningful ratio, as often seen at the beginning of R'(Ti) curves). As a
140 selection criterion, the R'(Ti) values should be fairly constant, although they often have a
141 small slope (<10%; S parameter, Table 1) due to the cooling rate effect on TRM acquisition,
142 which appears, based on our Triaxe experiments, to be weaker for magnetic grains with
143 lower unblocking temperatures (Le Goff and Gallet, 2004; see also Kostadinova-Avramova
144 and Jordanova, 2019; Schnepp et al., 2021). Hence, Triaxe archeointensity data are not
145 derived from the ratios between the NRM and TRM_{lab} fractions remaining between Ti and T2,
146 i.e., the R(Ti) dataset (Le Goff and Gallet, 2004). Doing so would enhance the influence of
147 the magnetic grains with high unblocking temperatures, leading to an increase of R(Ti) values
148 with temperature. Note, however, that for a relatively large number of fragments, the R(Ti)

149 data show only a weak increasing trend with temperature, indicating that the cooling rate
150 effect is often small or even negligible.

151 When a secondary magnetization component is detected from the thermal
152 demagnetization above T1, for instance, a partial TRM due to firing in a violently destructive
153 or, more simply, culinary, context, it is necessary to reduce the temperature range to one
154 between temperature T1' (>T1) and T2 so that the intensity determination is carried out only
155 on the primary magnetization acquired by an archeological artifact (Fig. 3, Table S1). An
156 important advantage of the Triaxe protocol is that the intensity values do not need to be
157 corrected for the anisotropy effect on TRM acquisition because the laboratory TRM is
158 acquired in a direction as close as possible to that of the NRM (e.g. Le Goff and Gallet,
159 2004). Moreover, acquiring a near-complete TRM_{lab} in a single heating step in place of the
160 NRM reduces the effect associated with the presence of multi-domain grains.

161

162 **3. The AutoR'(Ti) dataset, an additional parameter for Triaxe analysis**

163 Examination of the thermal demagnetization diagram obtained from Triaxe
164 measurements (M1 series) allows the different magnetization components carried by a
165 specimen to be distinguished, thus guiding the choice of the temperature interval from which
166 the R'(Ti) data will be taken in such a manner that that only the constant-direction fraction of
167 the NRM is involved in calculating a mean archeointensity value (Fig. 3). Interestingly, the
168 large number of measurements performed during the thermal demagnetization of the NRM
169 can reveal the cases in which the primary component is preserved only in the highest
170 temperature range, while a secondary component is largely predominant in the total
171 magnetization. This situation would probably be more difficult to capture with a stepwise
172 demagnetization performed every 25°C or 50°C.

173 The presence of a secondary magnetization component can also be demonstrated using
174 the set of mean R'(Ti) values obtained by gradually reducing the temperature range from
175 temperatures between T1 and T2 to temperatures only between T2-δT and T2, with δT ~50°C
176 (i.e., establishing a minimum of 10 data points with which to estimate the average R'(Ti)
177 value). Hereafter, T2- δT is referred to as T2'. The curve so obtained is called the AutoR'(Ti)
178 curve. The R'(Ti) and R(Ti) values are thus series of individual data at Ti, while the
179 AutoR'(Ti) values correspond to a series of R'(Ti) averages estimated over temperature
180 intervals beginning at Ti and ending at T2. Several examples for specimens from the Near
181 East are shown in Figures 4 and S1 (see details in the figure captions and Table S1). The
182 AutoR'(Ti) values increase from T1 (150°C) up to about 280°C-360°C, depending on the
183 specimens, and the values then stabilize for higher temperatures. Each stabilized segment
184 corresponds to the temperature range in which just the characteristic magnetization
185 component is isolated (in rare cases, the AutoR'(Ti) data show apparent oscillations, but these
186 have no particular significance). Between T1' and T2', the R'(Ti) and AutoR'(Ti) values are
187 very close to each other. The R(Ti) and AutoR'(Ti) curves also have similarities but the R(Ti)
188 curves are much less exploitable, in particular because of the cooling rate effect on TRM
189 acquisition (see below). We further note that in each case, every AutoR'(Ti) value for the
190 stabilized segment should ideally be associated with a weak slope (a maximum value of 10%
191 for the S parameter is used as a selection criterion for the R'(Ti)-based results; Table 1).
192 Nevertheless, it appears that slopes can be >10% at certain temperatures but this situation has
193 no significant impact on the overall evolution of the AutoR'(Ti) data. The most important
194 feature to check here is the stabilization of the AutoR'(Ti) values between T1' and T2' or at
195 least over a significant segment of this temperature interval (see below).

196 The results shown in Figures 4 and S1 indicate that there may be two possible ways to
197 determine a Triaxe archeointensity value for a specimen: 1) use the mean R'(Ti) value

198 between T1' and T2; and 2) average the AutoR'(Ti) values obtained between T1', or a
199 temperature close to T1', and T2' when these values are nearly constant. Our numerous
200 Triaxe measurements show that the results for (1) and (2) are fairly equivalent to within 1 or 2
201 μT, at most. In practice, however, while AutoR'(Ti) data are essential to determine the
202 temperature range over which a mean intensity value can be derived from the R'(Ti) data, the
203 use of AutoR'(Ti) data to calculate an archeointensity value may not prove to be so
204 straightforward (see Section 4). So far, we have utilized the first approach only and verified
205 that the temperature T1' derived from the thermal demagnetization diagram marks a
206 stabilization of the AutoR'(Ti) values. It is important to specify that specimens for which the
207 AutoR'(Ti) curve never stabilizes between T1' and T2' will be systematically rejected, even if
208 the R'(Ti) curve is substantially constant over this temperature range, because the average of
209 the R'(Ti) data then depends critically on the chosen temperature T1'. Non-stabilization may
210 occur for a variety of reasons, such as a large overlap of the demagnetization spectra of two
211 magnetization components (which should be detectable via thermal demagnetization
212 analysis), inappropriate behavior of the magnetic mineralogy, or, as we will see in Section 4,
213 the cooling rate effect on TRM acquisition. In the latter case, specific complementary
214 analyses can help to solve the problem.

215

216 **4. Cooling rate effect**

217 The Triaxe archeointensity results are considered to take the cooling rate effect on
218 TRM acquisition into account because the R'(Ti) parameter allows us to reduce the influence
219 of the magnetic grains most affected by this effect (Le Goff and Gallet, 2004). This cooling
220 rate effect can be further examined by comparing the intensity values obtained for different
221 cooling rates in TRM_{lab} acquisition. Such experiments, which can be performed on either true
222 archeological NRM or pseudo-NRM (i.e., a TRM acquired in known field and thermal

223 conditions), can thus be helpful in strengthening the R'(Ti)-derived intensity data routinely
224 acquired using a cooling rate of 25°C/minute. For instance, Salnaia et al. (2017) analyzed true
225 NRM from brick fragments from Novgorod, Northwestern Russia using two cooling rates
226 (25°C/minute and 2°C/minute). Below, we present other examples that make use of
227 AutoR'(Ti) data.

228 A pseudo-NRM of six baked-clay artifacts of different geographic origins and ages is
229 examined first (Fig. 5 and S2). The pseudo-NRM are acquired using a cooling rate of
230 2°C/minute at laboratory-field intensities varying between 35 μT and 75 μT. Analyses are
231 then performed between 150°C and ~500°C using cooling rates of 25°C/minute, 10°C/minute,
232 and 2°C/minute for TRM_{lab} acquisition. This sequence requires that the Triaxe be used for
233 four days for each specimen. Note that the constant laboratory cooling rate of 2°C/minute for
234 pseudo-NRM acquisition was not chosen to reproduce the original cooling rate (undoubtedly
235 not constant) that prevailed for true-NRM acquisition faithfully; rather, our experiments allow
236 for a better characterization of the cooling rate effect when (pseudo-)NRM and TRM_{lab} are
237 acquired under similar thermal conditions, the only difference being the constant cooling rates
238 applied. The R(Ti), R'(Ti), and AutoR'(Ti) datasets obtained for specimens from France,
239 Angkor (Cambodia), and Axum (Ethiopia), for which magnetization is mainly carried by
240 minerals from the magnetite family with various levels of impurities (Genevey et al., 2009;
241 2021 and in preparation), are shown in Figures 5 and S2 (other series of measurements, not
242 presented, give similar results). Two essential features of the Triaxe method are identified,
243 namely, the increase in the R(Ti) values with temperature (blue symbols filled with white)
244 while the R'(Ti) values (blue symbols) remain nearly constant over the entire temperature
245 range used for the intensity calculation. The increase in R(Ti) values depends on the
246 fragments, i.e. their variable cooling rate effects. As observed by Le Goff and Gallet (2004),
247 the increase in R(Ti) values slows when the cooling rate for TRM_{lab} acquisition approaches

248 the rate used for the pseudo-NRM acquisition. At the same time, the R'(Ti) values always
249 remain nearly constant, whatever the cooling rate, making impossible to detect a notable
250 (>5%) or systematic bias as a function of the cooling rate used (Table S1; recall that the
251 R'(Ti) values are averaged over the entire temperature range between T1 and T2, which
252 reduces the influence of a small shift towards the highest temperatures).

253 Contrary to the cases presented in Figure 4, an increase in AutoR'(Ti) values (red
254 symbols) with temperature is observed. In more detail, it can be seen that after a segment of
255 rather constant values, close to the R'(Ti) values, extending up to 300°C, sometimes to
256 350°C, the AutoR'(Ti) values increase significantly. Again, this increase depends on the
257 cooling rate for TRM_{lab} acquisition. This evolution is not surprising due to the definition of
258 the AutoR'(Ti) values, i.e., the more the temperature range used for their calculation shrinks
259 to high temperatures, the more the magnetic fraction involved is the one most affected by the
260 cooling rate effect. The AutoR'(Ti) data provides more information on the range of
261 unblocking temperatures for which the magnetic grains are minimally affected by the cooling
262 rate effect; in this regard, it seems that the limiting temperature is often close to 300°-350°C.
263 Thus, at this stage, it appears that the constancy of the AutoR'(Ti) values over the whole
264 temperature range used for the calculation of the R'(Ti) averages is not a determining
265 element; it appears to be more important to look for a constant evolution of these values over
266 a significant segment of temperatures above T1, i.e., over ~150-200°C (here, up to 300°C-
267 350°C), before an eventual inflection point is reached, signaling an increase over the highest
268 temperatures.

269 This point is further illustrated by the analysis of true archeological NRM. Figure 6
270 displays the data obtained for three pottery fragments sampled from the same archeological
271 context in the Near East. A specimen thermal demagnetization diagram is shown for each
272 fragment (left diagrams). For clarity, only the R'(Ti) (blue symbols; Table S1) and

AutoR'(Ti) (red symbols) data obtained from four specimens from the same fragment, analyzed with either a cooling rate of 25°C/minute (symbols filled with white) or 2°C/minute for TRM_{lab} acquisition, are reported on the right diagrams. In all but one case, the AutoR'(Ti) values show an inflection point around 300-350°C, before the beginning of an increasing trend. Before this inflection point, the R'(Ti) and AutoR'(Ti) data are close. Among the different AutoR'(Ti) curves, the one obtained for a specimen of fragment Lot31-01 shows neither stabilization nor inflection (red dots filled with white, Fig. 6b), making it impossible to determine a reliable archeointensity result from the R'(Ti) curve (the latter curve is thus missing from the corresponding figure, and the specimen must be rejected). As seen previously, using a cooling rate of 2°C/minute instead of 25°C/minute for the TRM_{lab} acquisition significantly dampens the increase in AutoR'(Ti) values. However, increases are still present, and sometimes shifted towards higher temperatures, indicating that the archeological cooling rate for these fragments was likely slower than 2°C/minute. Although making the AutoR'(Ti) data more difficult to exploit for the determination of quantitative intensity, these results show the reliability of the R'(Ti) values. However, we certainly cannot exclude the possibility that some specimens or fragments analyzed according to the Triaxe protocol could occasionally slightly overestimate archeointensity values (>5%; recall the slope for the R'(Ti) data). This uncertainty highlights the importance of studying several specimens per fragment from a group of several fragments taken from different artifacts found in the same archeological ensemble (the latter "overall" mean intensity value then being used for geomagnetic or archeological inferences). Still, a cooling rate of 10°C/minute, instead of 25°C/minute, could be used for TRM_{lab} acquisition. Even though any gain in reliability would be difficult to evaluate, this alternative does not pose a problem: the time needed to analyze a specimen would remain less than 3 hours and would not fundamentally change the "productivity" of a working day.

5. Discussion

The interpretation of the Triaxe measurements is based on several selection criteria (see Table 1). They are few in number because our approach remains relatively qualitative, relying on the results of numerous experiments conducted on various archeological artifacts. Indeed, not all the elements mentioned above are systematically quantified. This concerns the use of the AutoR'(Ti) data in particular, even though it is possible to calculate an average for these data over their stable segment. It is quite simple to deal with a stabilized segment that persists up to the highest temperature. When this is not the case, the calculation of the average of the AutoR'(Ti) values requires a precise determination of the temperature range used. This quantification leads to additional selection criteria with arbitrarily chosen threshold values of questionable efficiency. In our approach, the AutoR'(Ti) data are above all crucial to constrain the temperature interval over which to average the R'(Ti) data (i.e. the choice of temperature T1') or possibly reject the data. Nevertheless, we recognize that when Triaxe-type magnetometers become commercially available and the associated analysis method is commonly used by other research groups, these additional criteria will allow for better homogenization of Triaxe-derived archeointensity results. Currently, we use what appears to be the simplest method, one that takes into account the largest possible magnetization fractions and minimizes the cooling rate effect on TRM acquisition as much as possible. Note that the selection criteria used could lead to rejected fragments, for which a significant cooling rate effect would preferentially concern the magnetic grains with low or moderate unblocking temperatures. Another crucial condition, one that obviously impacts all intensity methods, is that any intensity determination for a specimen be performed on its primary (single-vector) magnetization. Finally, it is important to remember that the reliability of all our archeointensity results is constrained by consistency tests carried out both on each

fragment (now from a minimum of two specimens, often three studied per fragment, with a 5% limit around the average values) and a group of fragments coming from the same archeological context (with a minimum of three fragments and holding the standard deviation around the mean to less than 5 μT and 10%).

There are several possible approaches to select and use Triaxe intensity measurements. For the determination of an archeointensity value at the fragment level, it would, for instance, be possible to use an approach quite similar to that of Shaar et al. (2016), i.e., examine the averages of all combinations of the mean R'(Ti) data available for the different specimens (i.e., the AutoR'(Ti) data over their stabilized segment with, for each combination, a single mean R'(Ti) datum per specimen) with S and K parameters of less than 10% and greater than 50%, respectively. Here, we calculate the mean of all averages and the square root of the mean of all variances. This "global" approach relies on a large number of averages, generally more than several thousand, depending on the amount of AutoR'(Ti) data generated per specimen and the number of specimens per fragment, whereas the current method relies on a single average, i.e., a single AutoR'(Ti) datum at temperature T1', for each specimen. To illustrate the two options, a comparative test was performed for two groups of fragments from Tell Begum, Iraq (BG39-40; Gallet et al., 2021) and Qatna, Syria (SY03; Livermore et al., 2021). The results given in Table 2 (see the columns referred to as "Single average" and "All averages") show that the differences are within the error bars and can therefore be considered to be negligible.

Accordingly, using the two sets of means per fragment to derive a mean at the fragment group level yields statistically identical results (columns headed "Mean (1)" and "Mean (2)", Table 2). Furthermore, it is also possible to analyze the group means derived from all combinations of AutoR'(Ti) data from all specimens and fragments in the same group. These combinations are so numerous that it is necessary to randomly reduce their

number. This reduction was performed by taking into account the respective number of combinations between the different fragments. Doing so introduces a de facto weighting of the data, on the one hand, according to the number of specimens studied per fragment and, on the other hand, according to the temperature range selected for each specimen (the wider the range, the greater the number of AutoR'(Ti) values). Such calculations are tedious, but, in the end, the results are statistically identical to those obtained previously (column Mean (3), Table 2). When applied to a fragment, the global approach does introduce no, or very little, weighting according to the specimens because the temperature ranges selected for the different specimens are often very similar. At this stage, it thus appears that the simple method we have used so far (single average per fragment, then a single average of the fragment intensity values), plus consistency tests per fragment and per group of fragments, allows most of the (small) differences induced by the different options to be eliminated, making these options statistically equivalent.

It should be stressed that larger differences might occur in the estimation of the uncertainties in the means per fragment group. In the present case, as in our previous publications, these uncertainties are measured via the variance of the means per fragment, whereas a more complete calculation might also take into account the mean of all the variances per fragment, with the resulting variance being the sum of the two. For the Tell Begum data (Mean (1) and Mean (2); Table 2), the standard deviations would change from 1.2 μT and 1.1 μT to 1.3 μT and 1.4 μT, respectively, while the standard deviations of the group means from the Qatna-SY03 data would increase from 3.2 μT and 3.1 μT to 3.6 μT and 3.5 μT, respectively. For the latter calculations, the uncertainties of the R'(Ti) averages obtained per specimen were not taken into account; had they been used, Mean (1) for Tell Begum and Qatna would have been 34.7 ± 1.7 μT and 78.6 ± 3.7 μT, respectively. The simplicity of these calculations should allow them to be generalized, at least taking into

account the uncertainties in intensity values determined per fragment when estimating a mean value for a group of fragments.

Finally, the Triaxe magnetometer can be used for more than archeointensity determinations, as it can be used to test Thellier's laws (independence, reciprocity and additivity) for partial TRM or in an examination of the evolution of the magnetic viscosity as a function of temperature (see discussion in Le Goff et al., 2007). These application are outside the scope of this study because our focus remains on the archeointensity method initially developed by Le Goff and Gallet (2004), for which the reliability of the data is essentially verified by linearity criteria (i.e., by the stability of the ratio between the NRM and TRM_{lab} lost fractions as a function of temperature).

6. Concluding remarks

The archeointensity protocol developed specifically for the Triaxe magnetometer has proven to be effective and reliable, which does not preclude for further improvements, such as the one based on the AutoR'(Ti) data presented in this study. It has already been used in the acquisition of data in Western Europe, the Near East and Central Asia (Shaar et al., 2020; Genevey et al., 2021; Troyano et al., 2021). The Triaxe archeointensity data obtained in Western Europe, in particular, had led to the novel and intriguing observation of a ~260-year pseudo-periodicity in the occurrence of intensity peaks over the past 1700 years (Genevey et al., 2016, 2021; Livermore et al., 2018). These archeointensity studies have so far been the focus of Triaxe magnetometer use and we have not yet further explored the potential of this instrument for more focused studies on rock magnetism, i.e., on the fundamental properties of thermoremanent magnetization in baked clays and volcanic rocks (e.g. Coe et al., 2014). For volcanic rocks, the majority of the intensity tests performed to date have been disappointing, as most of the data gathered have been rejected on the basis of the selection criteria

established with baked clay artifacts, casting doubt on the predominantly thermoremanent nature of the magnetization carried by many volcanic rocks. With the increasing use of Triaxe-type magnetometers in the paleomagnetism community, there is no doubt that many studies will eventually focus on these aspects.

Acknowledgements

We thank two anonymous reviewers for their helpful comments on the manuscript.

References

Aitken, M. J., Allsop, A. L. , Bussell, G. D. , and Winter, M. B., 1988. Determination of the intensity of the Earth's magnetic field during archaeological times: Reliability of the Thellier technique. Rev. Geophys. 26, 3-12

Brown, M., Hervé, G., Korte, M., Genevey, A., 2021. Global archaeomagnetic data: the state-of-the-art and future challenges. Phys. Earth Planet. Inter., 318, 106766.

Boyd, M., 1986. A new method for measuring paleomagnetic intensities. Nature 319, 208-209.

Campuzano, S. A., Gómez-Paccard, M., Pavón-Carrasco, F. J., Osete, M. L., 2019. Emergence and evolution of the South Atlantic Anomaly revealed by the new paleomagnetic reconstruction SHAWQ2k. Earth Planet. Sci. Lett. 512, 17-26.

Coe, R. S., 1967. Paleo-intensities of the Earth's magnetic field determined from Tertiary and Quaternary rocks. J. Geophys. Res. 72, 3247–3262.

Coe, R. S., Jarboe, N. A., Le Goff, M., Petersen, N., 2014. Demise of the rapid-field-change hypothesis at Steens Mountain: The crucial role of continuous thermal demagnetization.

421 Earth Planet. Sci. Lett. 400, 302-312.

422 Constable, C., Korte, M., Panovska, S., 2016. Persistent high paleosecular variation activity in
423 southern hemisphere for at least 10000 years. Earth Planet. Sci. Lett. 453, 78–86.

424 Dunlop, D, Özdemir, Ö, 1997. Rock magnetism, Fundamental and Frontiers. Cambridge
425 Univ. Press, 573 pp.

426 Fox, J., Aitken, M., 1980. Cooling-rate dependence of thermoremanent magnetization. Nature
427 283, 462-463.

428 Gallet, Y., Genevey, A., Le Goff, M., Fluteau, F., Eshragi, S. A., 2006. Possible impact of the
429 Earth's magnetic field on the history of ancient civilizations. Earth Planet. Sci. Lett.
430 246, 17-26.

431 Gallet, Y., D'Andrea, M., Genevey, A., Pinnock, F., Le Goff, M., Matthiae, P., 2014.
432 Archaeomagnetism at Ebla (Tell Mardikh, Syria). New data on geomagnetic field
433 intensity variations in the Near East during the Bronze Age. J. Archaeol. Sci. 42, 295-
434 304.

435 Gallet, Y., Molist, M., Genevey, A., Clop Garcia, X., Thébault, E. Gómez Bach, A., Le Goff,
436 M. Robert, B., Nachasova, I., 2015. New Late Neolithic (c. 7000–5000 BC)
437 archeointensity data from Syria. Reconstructing 9000 years of archeomagnetic field
438 intensity variations in the Middle East. Phys. Earth Planet. Inter. 238, 89-103.

439 Gallet, Y., Fortin, M., Fournier, A., Le Goff, M., Livermore, P., 2020. Analysis of
440 geomagnetic field intensity variations in Mesopotamia during the third millennium BC
441 with archeological implications. Earth Planet. Sci. Lett. 537, 116183.

442 Gallet, Y., Fournier, A., Livermore, P.W., 2021. Tracing the geomagnetic field intensity
443 variations in Upper Mesopotamia during the Pottery Neolithic to improve ceramic-
444 based chronologies. J. Archaeol. Sci. 132, 105430.

445 Genevey, A., Gallet, Y., 2002. Intensity of the geomagnetic field in western Europe over the
446 past 2000 years: new data from ancient French pottery. J. Geophys. Res. 107 (B11),
447 2285.

448 Genevey, A., Gallet, Y., Margueron, J.-C., 2003. Eight thousand years of geomagnetic field
449 intensity variations in the eastern Mediterranean. J. Geophys. Res. 108 (B5), 2228.

450 Genevey, A., Gallet, Y., Constable, C., Korte, M., Hulot, G., 2008. ArcheoInt: An upgraded
451 compilation of geomagnetic field intensity data for the past ten millennia and its
452 application to the recovery of the past dipole moment. Geochem. Geophys. Geosys.
453 9(4), Q04038.

454 Genevey, A., Gallet, Y., Rosen, J., Le Goff, M., 2009. Evidence for rapid geomagnetic field
455 intensity variations in Western Europe over the past 800 years from new archeointensity
456 French data. Earth Planet. Sci. Lett. 284, 132–143.

457 Genevey, A., Gallet, Y., Thébault, E., Jesset, S., Le Goff, M., 2013. Geomagnetic field
458 intensity variations in Western Europe over the past 1100 years. Geochem. Geophys.
459 Geosyst. 14/8, 2858–2872.

460 Genevey, A., Gallet, Y., Jesset, S., Thébault, E., Bouillon, J., Lefèvre, A., Le Goff, M., 2016.
461 New archeointensity data from French Early Medieval pottery production (6th–10th
462 century AD). Tracing 1500 years of geomagnetic field intensity variations in Western
463 Europe. Earth Planet. Sci. Lett. 257, 205-219.

464 Genevey, A., Gallet, Y., Thébault, E., Livermore, P. W., Fournier, A., Jesset, S., Lefèvre, A.,
465 Mahé-Hourlier, N., Marot, E., Regnard, S., 2021. Archeomagnetic intensity
466 investigations of French medieval ceramic workshops: Contribution to regional field
467 modeling and archeointensity dating. Phys. Earth Planet. Inter. 318, 106750.

Hartmann, G.A., Genevey, A., Gallet, Y., Trindade, R.I.F., Etchevarne, C., Le Goff, M., Afonso, M.C., 2010. Archeointensity in Northeast Brazil over the past five centuries. Earth Planet. Sci. Lett. 296, 340–352.

Hartmann, G., Genevey, A., Gallet, Y., Trindade, R., Le Goff, M., Najjar, R., Etchevarne, C., Afonso, M., 2011. New historical archeointensity data from Brazil : Evidence for a large regional non-dipole field contribution over the past few centuries. Earth Planet. Sci. Lett. 306, 66-76.

Hellio, G., Gillet, N., 2018. Time-correlation based regression of the geomagnetic field from archeological and sediment records. Geophy. J. Int. 214 (3), 1585-1607.

Hervé, G., Fassbinder, J., Gilder, S., Metzner-Nebelsick, C., Gallet, Y., Genevey, A., Schnepp, E., Geisweid, L., Pütz, A., Reub, S., Wittenborn, F., Flontas, A., Linke, R., Riedel, G., Walter, F., Westhausen, I., 2017. Fast geomagnetic field intensity variations between 1400 and 400 BCE: new archaeointensity data from Germany. Phys. Earth Planet. Inter. 270, 143-156.

Hervé, G., Perrin, M., Alva-Valdivia, L., Tchibinda, B. M., Rodriguez-Trejo, A., Hernandez-Cardona, A., Cordóva Tello, M., 2019a. Critical analysis of the Holocene palaeointensity database in Central America : Impact on geomagnetic modelling. Phys. Earth Planet. Inter. 289, 1-10.

Hervé, G., Chauvin, A., Lanos, P., Rochette, P., Perrin, M., Perron d'Arc, M., 2019b. Cooling rate effect on thermoremanent magnetization in archaeological baked clays: an experimental study on modern bricks. Geophys. J. Int. 217 (2), 1413–1424.

Kostadinova-Avramova, M., Jordanova, N., 2019. Study of cooling rate effect on baked clay materials and its importance for archaeointensity determinations. Phys. Earth Planet. Inter. 288, 9-25.

Le Goff, M., Gallet, Y., 2004. A new three-axis vibrating sample magnetometer for continuous high-temperature magnetization measurements: applications to paleo- and archeo-intensity determinations. Earth Planet. Sci. Lett. 229, 31-43.

Le Goff, M., Gallet, Y., Genevey, A., 2007. Potential of high-temperature magnetization measurements for archeo- and paleo-intensity studies. European Geosciences Union, General Assembly, A-06820 MPRG04-1, Vienna (Austria) 15-20 April 2007.

Lhuillier, F., Shcherbakov, V. P., Shcherbakova, V. V., Ostner, S., Hervé, G., Petersen, N., 2019. Palaeointensities of Oligocene and Miocene volcanic sections from Ethiopia: field behaviour during the Cainozoic. Geophys. J. Int. 216, 1482-1494.

Livermore, P.W., Fournier, A., Gallet, Y., Bodin, T., 2018. Transdimensional inference of archeomagnetic intensity change. Geophys. J. Int. 215, 2008-2034.

Livermore, P.W., Gallet, Y., Fournier, A., 2021. Archeomagnetic intensity variations during the era of geomagnetic spikes in the Levant. Phys. Earth Planet. Inter. 312, 106657.

Licht, A., Hulot, G., Gallet, Y., Thébault, E., 2013. Ensembles of low degree archeomagnetic field models for the past three millennia. Phys. Earth Planet. Inter. 224, 38–67.

Paterson, G. A., L. Tauxe, L., A. J. Biggin, A. J., Shaar, R., and L. C. Jonestrask, L. C., 2014. On improving the selection of Thellier-type paleointensity data. Geochem. Geophys. Geosyst. 15(4), 1180-1192.

Pavón-Carrasco, F. J., Campuzano, S. A., Rivero-Montero, M., Molina-Cardín, A., Gómez-Paccard, M., & Osete, M.L., 2021. SCHA.DIF.4k: 4,000 years of paleomagnetic reconstruction for Europe and its application for dating. J. Geophys. Res. Solid Earth 126, e2020JB021237.

514 Poidras, T., Camps, P., Nicol, P. (2009). Controlled atmosphere vibrating thermo-
515 magnetometer (C_{at}VSM): a new device to optimize the absolute paleointensity
516 determinations. Earth Planets Space 61, 101-110.

517 Salnaia, N., Gallet, Y., Genevey, A., Antipov, I., 2017. New archeointensity data from
518 Novgorod (North-western Russia) between c. 1100 and 1700 AD. Implication for the
519 European intensity secular variation. Phys. Earth Planet. Inter. 269, 18-28.

520 Schnepp, E., Thallner, D., Arneitz, P., Leonhardt, R., 2021. New archeomagnetic secular
521 variation data from central Europe, II: Intensities. Phys. Earth Planet. Inter. 309,
522 106605.

523 Shaar, R., Tauxe, L., Ron, H., Ebert, Y., Zuckerman, S., Finkelstein, I., Agnon A., 2016.
524 Large geomagnetic field anomalies revealed in Bronze to Iron Age archeomagnetic data
525 from Tel Megiddo and Tel Hazor, Israel. Earth Planet. Sci. Lett. 442, 173-185.

526 Shaar, R., Bechar, S., Finkelstein, I., Gallet, Y., Martin, M. A. S., Ebert, Y., Keinan, J.,
527 Gonen, L., 2020. Synchronizing geomagnetic field intensity records in the Levant
528 between the 23rd and 15th centuries BCE: chronological and methodological
529 implications. Geochem. Geophys. Geosyst. 21, e2020GC009251.

530 Thellier, E., Thellier, O., 1959. Sur l'intensité du champ magnétique terrestre dans le passé
531 historique et géologique. Ann. Geophys. 15, 285–376.

532 Troyano, M., Gallet, Y., Genevey, A., Pavlov, V., Fournier, A., Lagroix, F., Niyazova, M.,
533 Mirzaakhmedov, D., 2021. Analyzing the geomagnetic axial dipole field moment over
534 the historical period from new archeointensity results at Bukhara (Uzbekistan, Central
535 Asia). Phys. Earth Planet Inter. 310, 106633.

536 Wilson, R. L. (1961). Palaeomagnetism in Northern Ireland. Part I. The thermal
537 demagnetization of natural magnetic moments in rocks. Geophys. J.R. Astron. Soc. 5,
538 45-58.

539 Yu, Y., Tauxe, L., Genevey, A., 2004. Toward an optimal geomagnetic field intensity
540 determination technique. Geochem. Geophys. Geosyst. 5, Q02H07.

541

542

543 **Figure captions**

544

545 **Fig. 1.** Photo of the three Triaxe magnetometers available at IPGP and LAMS. Their builder,
546 Maxime Le Goff, stands in front of them. @Yves Gallet

547 **Fig. 2.** Series of measurements carried out using the Triaxe archeointensity protocol
548 developed by Le Goff and Gallet (2004). The data are from specimen IR11-02x from
549 Susa, Iran (Shaur Palace of Artaxerxes II; Gallet et al., 2006 and unpublished). The
550 laboratory field for TRM_{lab} acquisition was set at 65 μT, higher than the archeointensity
551 in order to properly discriminate between the M1 and M5 series of measurements in the
552 diagram. In addition, the measurements acquired during the last cooling of the specimen
553 between T2 and room temperature have been omitted.

554 **Fig. 3.** Thermal demagnetization data obtained for specimen BG39-21c (left panel; Tell
555 Begum; Gallet et al., 2021) and the associated R'(Ti) values from T1 and T1' to T2
556 (right panel).

557 **Fig. 4.** Thermal demagnetization, R'(Ti), R(Ti) and AutoR'(Ti) data obtained for two
558 specimens from the Near East: a) Susa, Iran (unpublished); and b) Tell Brak, Syria
559 (unpublished). The left panels show the demagnetization diagrams. The right panels
560 exhibit the R(Ti) and R'(Ti) data between T1 and T2 (black filled with grey and blue
561 filled with white dots, respectively), the R'(Ti) data between T1' and T2 (blue dots),
562 and the AutoR'(Ti) data between T1 and T2' (=T2-~50°C) (red dots).

563 **Fig. 5.** Triaxe pseudo-NRM analyses of three different baked-clay artifacts. a) a specimen
564 from Chaudry, France (Genevey et al., 2021); b) a specimen from a temple in Angkor,

Cambodia (data not yet published); and c) a specimen from Axum, Ethiopia (data not yet published). The laboratory field intensities used for pseudo-NRM acquisition were 75 μT (a), 35 μT (b) and 40 μT (c), while a cooling rate of 2°C/minute was used in all cases. Each diagram includes the R(Ti), R'(Ti), and AutoR'(Ti) datasets (blue filled with white, blue and red symbols, respectively) obtained using successively cooling rates of 25°C/minute (dots), 10°C/minute (triangles), and 2°C/minute (inverted triangles).

Fig. 6. Triaxe analyses of the true archeological NRM of four specimens from three different fragments from the same archeological context sampled in the Near East (Lot31; Tell Sheikh Hamad, Northeastern Syria). Examples of the thermal demagnetization of one specimen taken from each fragment are shown in Fig. 6a (Lot31-01c), Fig. 6c (Lot31-04b), and Fig. 6e (Lot31-05b). In the diagrams to the right, the R'(Ti) (blue symbols) and AutoR'(Ti) (red symbols) datasets for the different specimens taken from their respective fragments using a cooling rate of 25°C/minute (symbols filled with white) and 2°C/minute are reported, with two specimens analyzed for each cooling rate: Fig. 6b, Fragment Lot31-01; Fig. 6d, Fragment Lot31-04; Fig. 6f, Fragment Lot31-05.

Fig. S1. Thermal demagnetization, R'(Ti), R(Ti) and AutoR'(Ti) data obtained from two additional specimens from Syria (see also Fig. 4): a) Tell Halula (Gallet et al., 2015); and b) Tell Atij (Gallet et al., 2020). The two left panels show the demagnetization diagrams. The right panels exhibit the R(Ti) and R'(Ti) data between T1 and T2 (black filled with grey and blue filled with white dots, respectively), the R'(Ti) data between T1' and T2 (blue dots), and the AutoR'(Ti) data between T1 and T2' (=T2-~50°C) (red dots).

Fig. S2. Triaxe pseudo-NRM analysis of three additional baked-clay artifacts (see Fig. 5): a) a specimen from Hospices de Beaune, France (Genevey et al., 2009); b) a specimen from

a temple in Angkor, Cambodia (not yet published); c) a specimen from Axum, Ethiopia (not yet published). The laboratory field intensities used for pseudo-NRM acquisition were 55 μT (a) and 40 μT (b), (c), while a cooling rate of 2°C/minute was used in all cases. Each diagram includes the R(Ti), R'(Ti), and AutoR'(Ti) datasets (blue filled with white, blue and red symbols, respectively) obtained using successively cooling rates of 25°C/minute (dots), 10°C/minute (triangles), and 2°C/minute (inverted triangles).

Table 1. Selection criteria used for the interpretation of the Triaxe intensity measurements. Some remarks on these criteria are also provided.

Table 2. Comparisons between the mean archeointensity values obtained at the fragment level and at the fragment-group level for two ensembles of potsherds collected at Tell Begum (BG39-40; Gallet et al., 2021) and Qatna (group SY03; Livermore et al., 2021) using two different approaches. An intensity value was obtained at the specimen level by averaging the R'(Ti) data (fourth column). A mean intensity value was derived at the fragment level either by averaging the previous specimen-mean intensity values (fifth column, which is headed "single average (1)") or by considering all combinations of the AutoR'(Ti) values available for the different specimens (sixth column, which is headed "All averages (2)"). The seventh and eighth columns report the mean values determined at the fragment-group level using the means given in the fifth and sixth columns, respectively. The last (ninth) column reports the group mean values obtained from a very large set of combinations of AutoR'(Ti) values from all specimens and fragments within the same group.

Table S1. Archeointensity results obtained from the R'(Ti) data shown in Fig. 3, 4, 5, 6, S1 and S2. For the data presented in Fig. 5 and S2 obtained from pseudo-NRM analyses using different cooling rates for TRM_{lab} acquisition, the differences from the applied

615 laboratory field intensity are also given in % (right column). See text and Table 1 for
616 the definition of the different parameters T1'-T2, K, S.

617

Figure 1

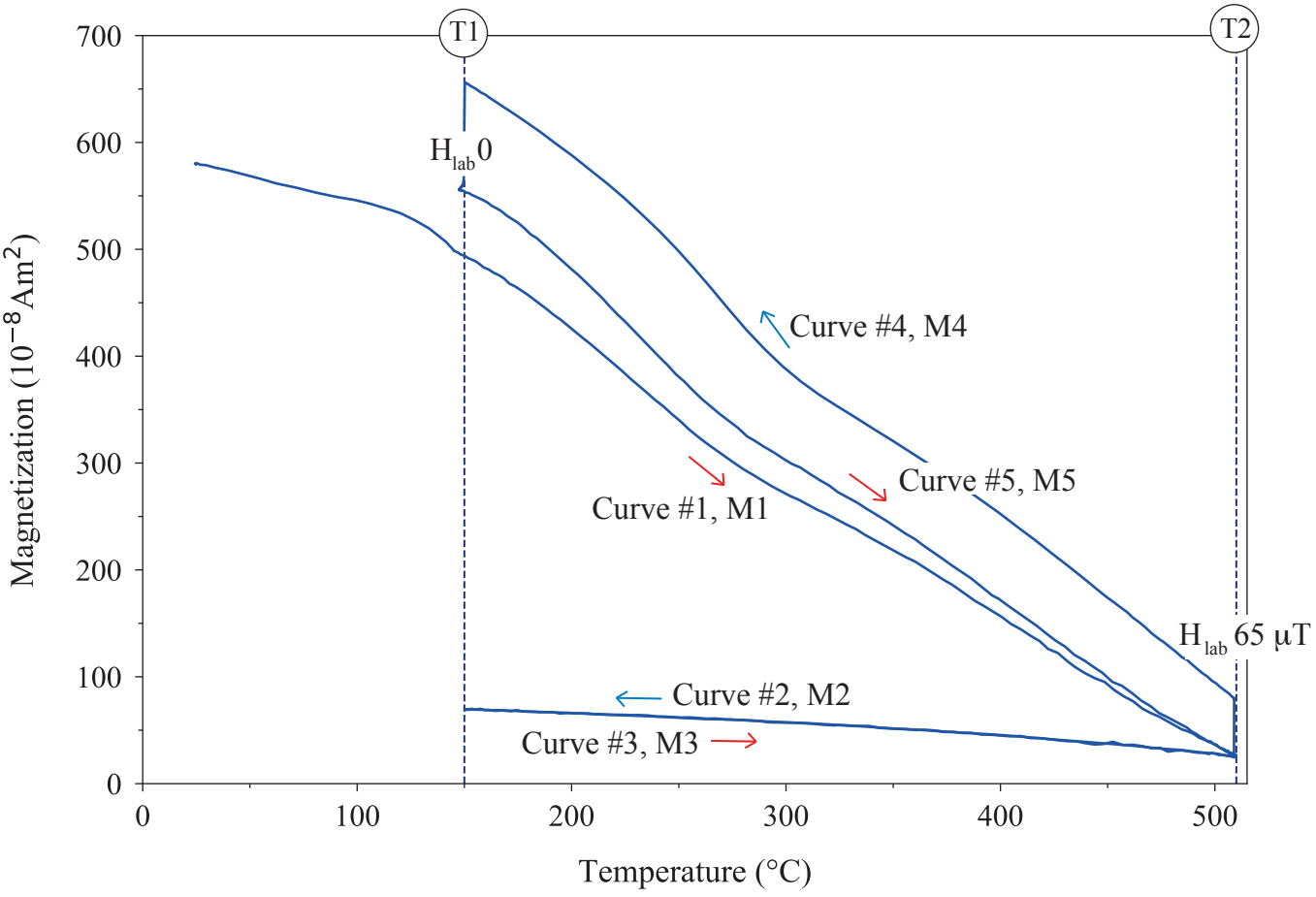
T1
T2
700
600
500
400
300
200
100
0
0
100
200
300
400
500
Magnetization (10^{-8}Am^2)
Temperature (°C)
H_{lab} 0
H_{lab} 65 μT
Curve #4, M4
Curve #5, M5
Curve #1, M1
Curve #2, M2
Curve #3, M3

Figure 2

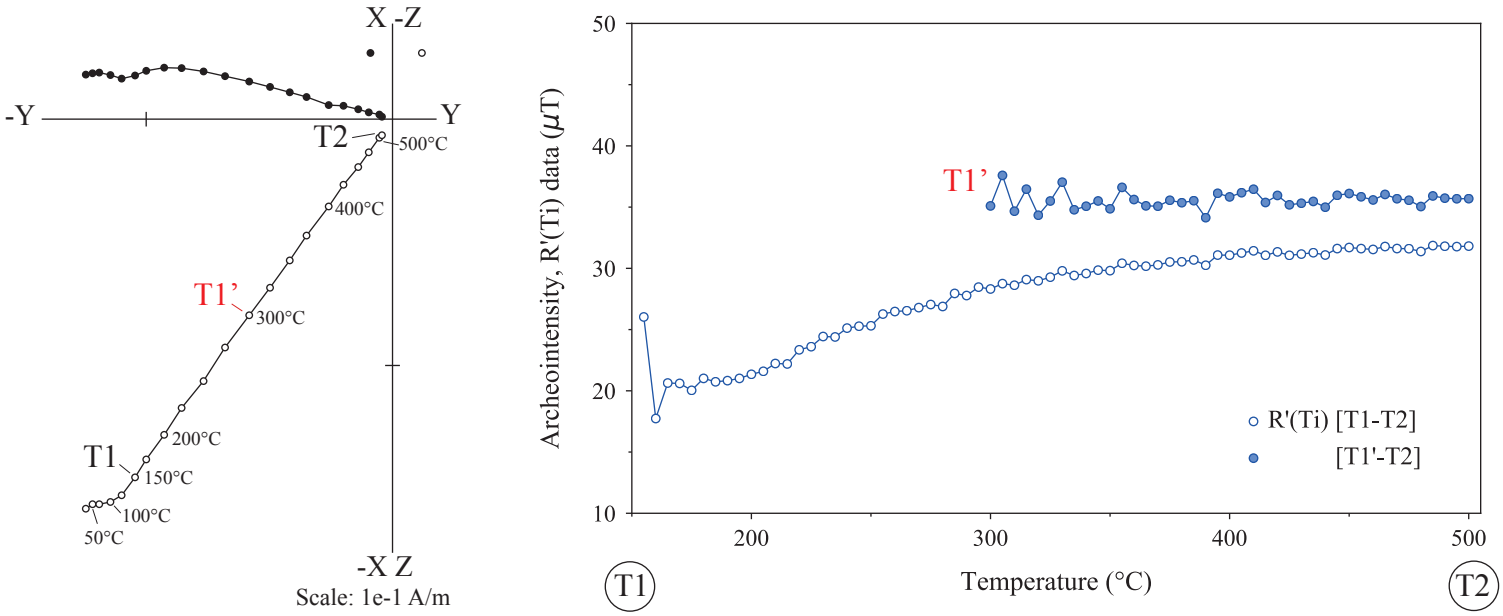
X -Z
-Y
Y
T2
500°C
400°C
T1'
300°C
200°C
T1
150°C
100°C
50°C
-X Z
Scale: 1e-1 A/m
Archeointensity, R'(Ti) data (μT)
50
40
30
20
10
T1'
R'(Ti) [T1-T2]
[T1'-T2]
200
300
400
500
Temperature (°C)
T1
T2

Figure 3

a) IR10-04b

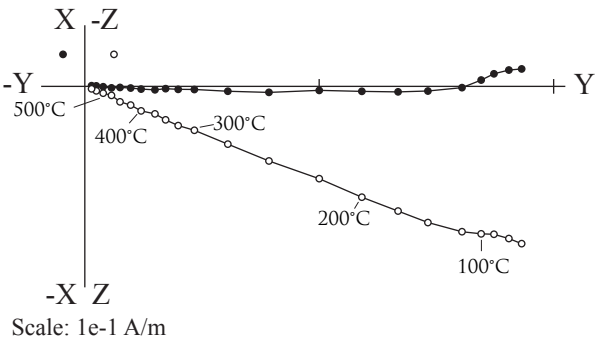

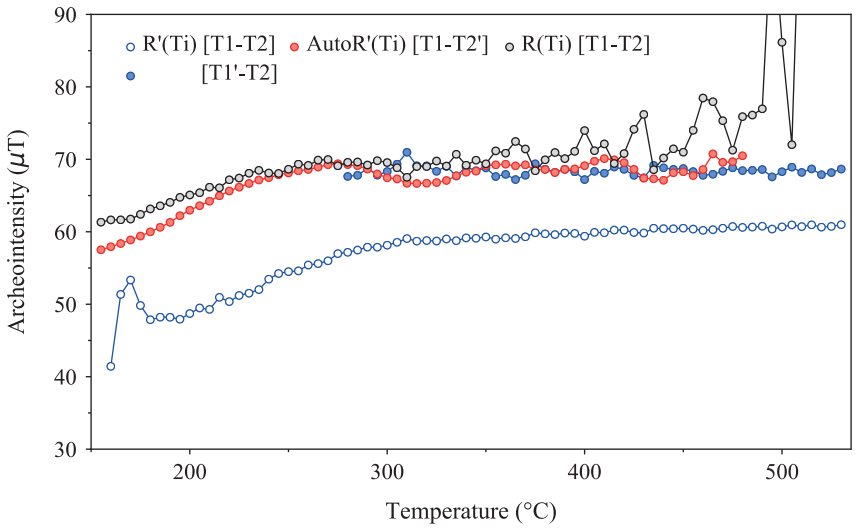

b) TB03-03b

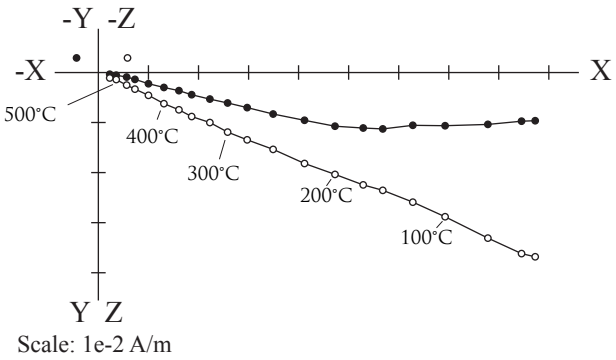

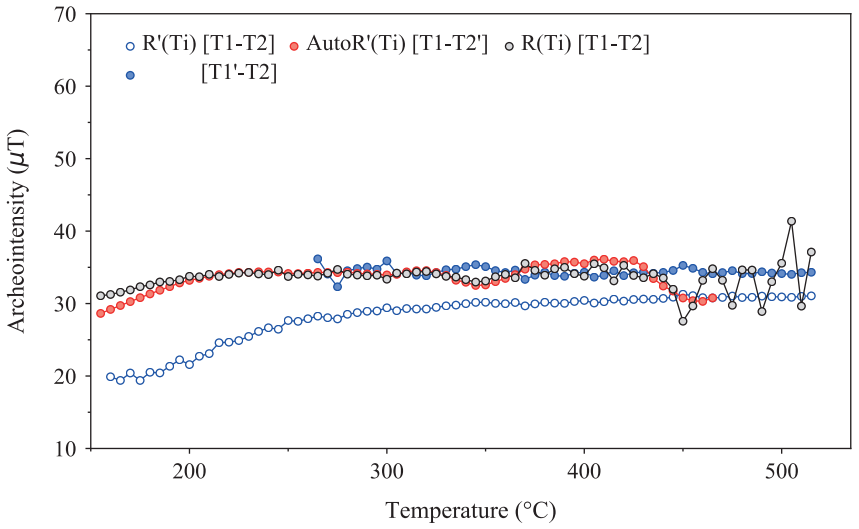

Figure 4

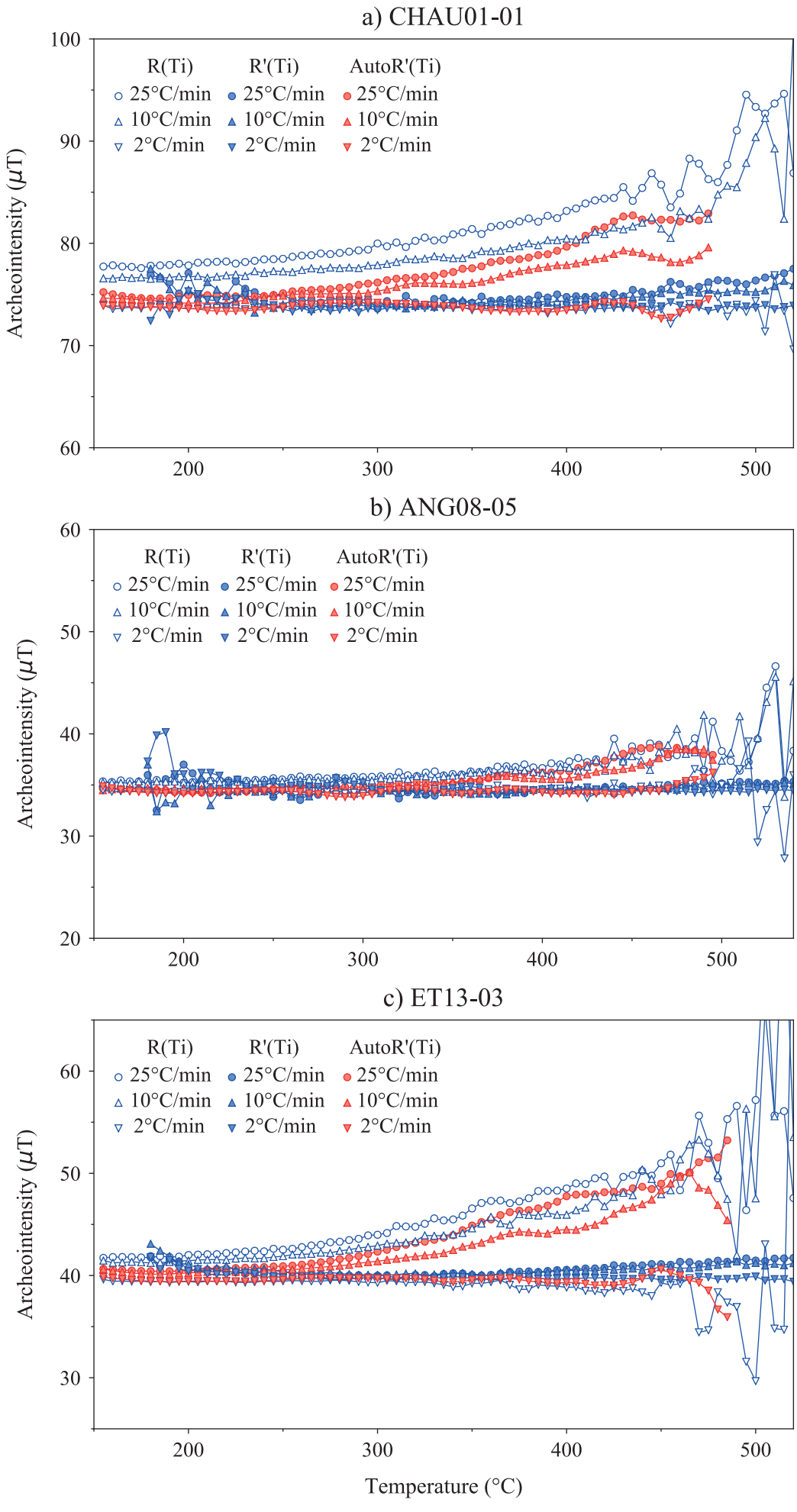
a) CHAU01-01
b) ANG08-05
c) ET13-03
R(Ti)
R'(Ti)
AutoR'(Ti)
25°C/min
10°C/min
2°C/min
Archeointensity (μT)
Temperature (°C)

Figure 5

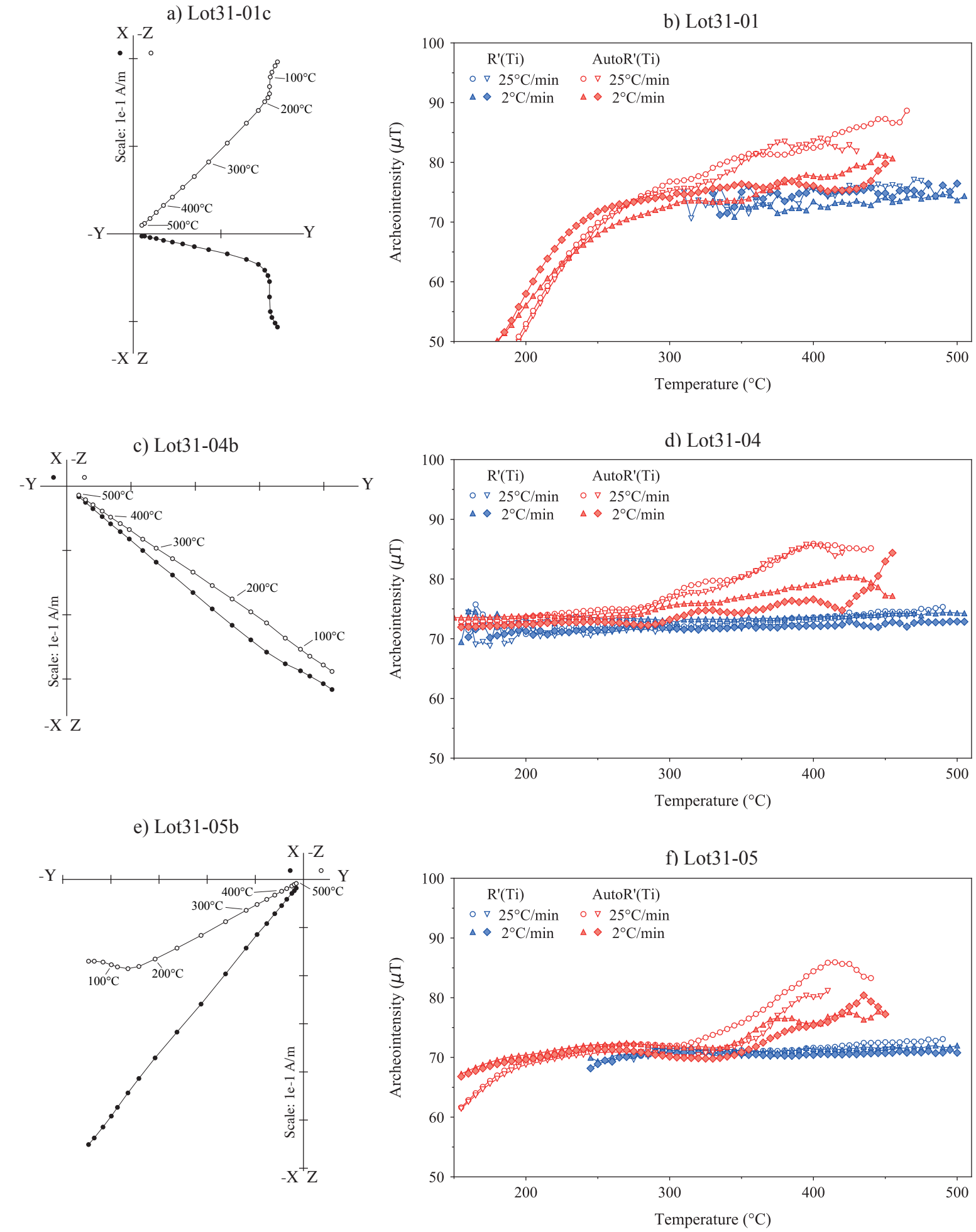
a) Lot31-01c
X -Z
-Y
Y
-X Z
Scale: 1e-1 A/m
100°C
200°C
300°C
400°C
500°C
b) Lot31-01
R'(Ti)
AutoR'(Ti)
25°C/min
2°C/min
Archeointensity (μT)
Temperature (°C)
c) Lot31-04b
d) Lot31-04
e) Lot31-05b
f) Lot31-05

Figure 6

An archeointensity value at the specimen level is obtained by averaging the R'(Ti) values over the temperature range, between T1' (or T1) and T2, where only the magnetization component acquired during the firing of the analyzed artifact is isolated. These R'(Ti) values must be substantially constant: their evolution as a function of temperature is approximated by a straight line whose slope (referred to as S parameter) must not exceed 10%.

Remark: in practice, we seek as much as possible a temperature interval allowing to obtain a slope of the order of 5%, or less, which remains as close as possible to the temperature range given by the analysis of the thermal demagnetization diagram. The almost constant values of R'(Ti) must be associated with R(Ti) values that progressively increase with temperature. This increase induced by the cooling rate effect on TRM acquisition varies according to the specimens analyzed. Note that in many cases, the R(Ti) values increase only little.

The fraction of magnetization between temperatures T1 (or T1') and T2 must be greater than or equal to 50% of the magnetization remaining at T1 (or T1'). It is referred to as the K parameter. It is estimated after subtracting the effect of the thermal variation of the magnetic fraction remaining blocked at T2 from the magnetization isolated between T1 (or T1') and T2.

Remark: this criterion is different from the one generally used for other paleointensity methods, which implies that an intensity value can only be retained if the magnetization fraction represents more than 50% of the total magnetization carried by the sample. This difference is justified by the large number of magnetization measurements (several dozen) performed between T1 (or T1') and T2 in the Triaxe procedure.

The AutoR'(Ti) values must be substantially constant and close to the R'(Ti) values over a significant temperature range (on the order of 150-250°C) above T1', or even in the most favorable cases over the entire temperature range between T1' and T2' (=T2-~50°C), with the S parameter ideally fluctuating below 10%.

Remark: reducing the selection of accepted data to only those specimens meeting the latter case would lead to the unnecessary rejection of a large number of specimens. On another hand, if the AutoR'(Ti) data are almost constant over the T1'-T2' temperature range, then the R(Ti) data must also be quasi constant, and both datasets must be close to the R'(Ti) data.

The above characteristics established for baked-clay artifacts define a standard magnetic behavior obtained when the magnetic mineralogy of the specimens studied does not alter (or very little) during the thermal treatment. Nevertheless, this absence of significant alteration must be confirmed by magnetic susceptibility measurements during heating: these must be reversible up to temperature T2.

Remark: One of the advantages of the Triaxe protocol is that it minimizes the heating time and the number of heating experienced by the specimen.

Table 1

Archeol. site/group	Fragment	Specimen	F specimen ± σ (μT)	F frag ± σ (μT) Single average (1)	F frag ± σ (μT) All averages (2)	F group ± σ (μT) Mean (1)	F group ± σ (μT) Mean (2)	F group ± σ (μT) Mean (3)
Tell Begum	**BG39-21**	BG39-21b	35.0 ± 0.3	35.3 ± 0.3*	35.3 ± 0.6			
		BG39-21c	35.6 ± 0.7					
	BG39-27	BG39-27a	34.4 ± 1.0	33.3 ± 1.1	32.4 ± 1.3			
		BG39-27b	32.2 ± 1.1					
		BG39-27c	33.3 ± 1.1					
	BG40-27	BG40-27a	32.7 ± 0.8	32.3 ± 0.5	33.2 ± 0.8			
		BG40-27b	32.5 ± 0.9					
		BG40-27c	31.7 ± 1.3					
	BG40-29	BG40-29a	33.1 ± 1.1	33.6 ± 0.4	33.8 ± 0.8			
		BG40-29b	33.9 ± 1.4					
		BG40-29c	33.7 ± 1.7					
	BG40-31	BG40-31a	32.7 ± 0.9	32.5 ± 0.3*	32.9 ± 0.7			
		BG40-31c	32.2 ± 0.6					
						33.4 ± 1.2	**33.5 ± 1.1**	**33.5 ± 1.2**
SY03, Qatna	**SY03-01**	SY03-01a	83.2 ± 1.8	79.6 ± 1.9	81.8 ± 2.2			
		SY03-01b	78.3 ± 1.3					
		SY03-01c	79.7 ± 1.4					
		SY03-01d	78.5 ± 1.4					
		SY03-01e	78.4 ± 1.4					
		SY03-01f	79.7± 1.5					
	SY03-03	SY03-03a	72.7 ± 1.0	73.8 ± 1.5	75.3 ± 1.5			
		SY03-03b	76.0 ± 0.6					
		SY03-03c	74.3 ± 0.9					
		SY03-03d	73.5 ± 1.2					
		SY03-03e	71.9 ± 0.8					
		SY03-03f	74.3 ± 1.3					
	SY03-04	SY03-04a	80.2 ± 1.8	80.0 ± 0.9	81.8 ± 1.5			
		SY03-04b	81.3 ± 1.3					
		SY03-04c	79.6 ± 1.3					
		SY03-04d	78.6 ± 1.2					
		SY03-04e	80.2 ± 1.3					
		SY03-04f	80.1 ± 1.1					
	SY03-06	SY03-06a	82.8 ± 1.1	80.8 ± 1.8	80.5 ± 1.6			
		SY03-06b	80.2 ± 0.5					
		SY03-06c	82.3 ± 0.3					
		SY03-06d	80.9 ± 0.6					
		SY03-06e	77.6 ± 0.5					
		SY03-06f	80.9 ± 0.6					
						78.6 ± 3.2	**79.9 ± 3.1**	**79.8 ± 3.1**

(* half difference)

Table 2

a) SY140-13

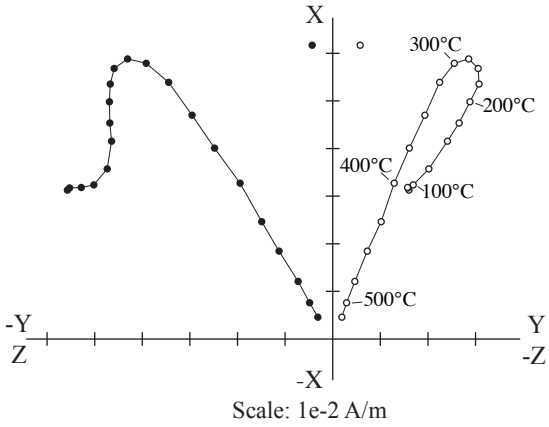

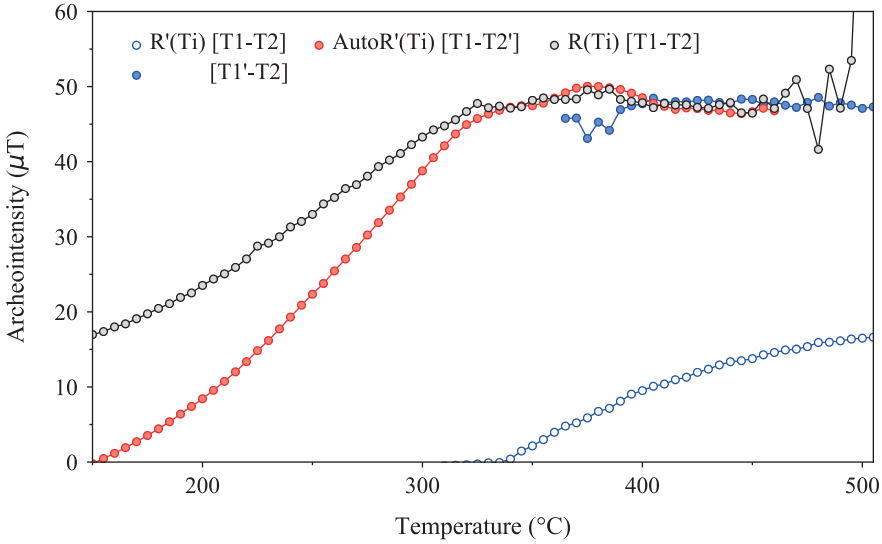

b) AT01-01a

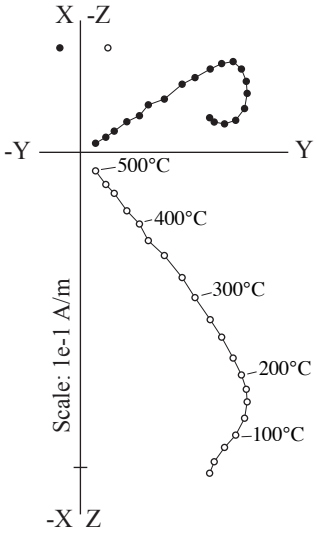

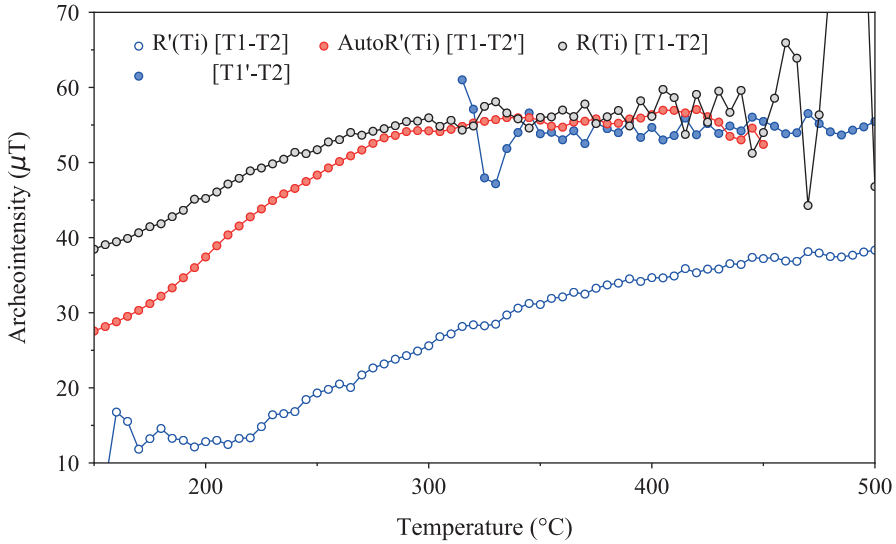

Figure S1

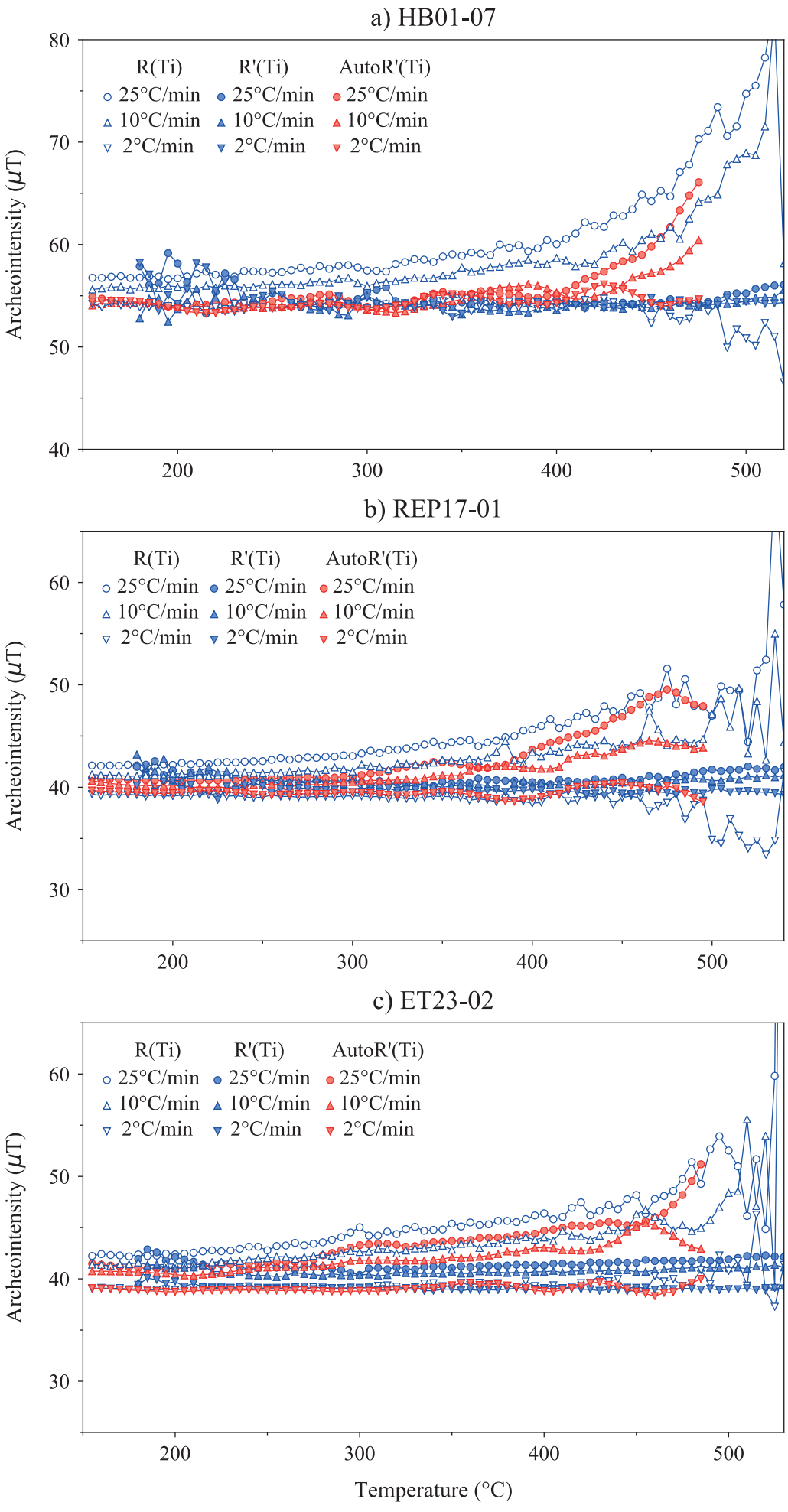
a) HB01-07
b) REP17-01
c) ET23-02
R(Ti)
R'(Ti)
AutoR'(Ti)
25°C/min
10°C/min
2°C/min
Archeointensity (μT)
Temperature (°C)

Figure S2

Figure		Fragment	Specimen	H_{Lab} (μT)	Cooling rate for TRM-lab acquisition (°C/Minute)	T1'-T2	K (%)	Slope S (%)	$F_{specimen}$ ± σ (μT)
Figure 3		**BG39-21**	BG39-21c	35	25	320-510	86	1	35.6 ± 0.7
Figure 4	**a)**	**IR10-04**	IR10-04b	65	25	280-530	92	0	68.4 ± 0.7
	b)	**TB03-03**	TB03-03b	35	25	265-515	89	-1	34.4 ± 0.6
Figure 5	**a)**	**CHAU01-01**	Same specimen analyzed sequentially	75	25	180-525	87	2	75.2 ± 0.9 (0.3%)
				75	10	180-525	87	1	74.7 ± 0.8 (-0.4%)
				75	2	180-525	86	0	73.8 ± 0.4 (-1.6%)
	b)	**ANG08-05**	Same specimen analyzed sequentially	35	25	180-545	96	1	34.7 ± 0.6 (-0.9%)
				35	10	180-545	96	3	34.5 ± 0.6 (-1.4%)
				35	2	180-545	96	-6	34.9 ± 1.0 (-0.3%)
	c)	**ET13-03**	Same specimen analyzed sequentially	40	25	180-535	95	3	40.7 ± 0.6 (1.8%)
				40	10	180-535	95	0	40.6 ± 0.6 (1.5%)
				40	2	180-535	95	-2	39.8 ± 0.4 (-0.5%)
Figure 6	**b)**	**Lot31-01**	Lot31-01b	75	25	-	-	-	-
			Lot31-01c	75	25	310-480	81	7	74.4 ± 1.6
			Lot31-01d	75	2	330-505	87	3	73.3 ± 1.0
			Lot31-01e	75	2	330-500	84	3	74.8 ± 1.2
	d)	**Lot31-04**	Lot31-04b	75	25	180-490	87	5	72.9 ± 1.1
			Lot31-04c	75	25	180-470	81	5	72.0 ± 1.1
			Lot31-04d	75	2	180-505	93	2	73.5 ± 0.5
			Lot31-01e	75	2	180-505	90	3	71.9 ± 0.6
	f)	**Lot31-05**	Lot31-05b	75	25	275-490	88	3	71.7 ± 0.7
			Lot31-05c	75	25	275-460	85	1	70.6 ± 0.4
			Lot31-05d	75	2	245-500	91	2	71.2 ± 0.6
			Lot31-05e	75	2	245-500	91	2	70.5 ± 0.5
Figure S1	**a)**	**SY140-13**	SY140-13	45	25	365-510	81	6	47.3 ± 1.3
	b)	**AT01-01**	AT01-01a	50	25	315-500	81	3	54.3 ± 2.2
Figure S2	**a)**	**HB01-07**	Same specimen analyzed sequentially	55	25	180-525	97	-2	54.9 ± 1.1 (-0.2%)
				55	10	180-525	97	1	54.1 ± 0.6 (-1.6%)
				55	2	180-525	96	-3	54.5 ± 1.0 (-0.9%)
	b)	**REP17-01**	Same specimen analyzed sequentially	40	25	180-545	97	1	40.9 ± 0.5 (2.3%)
				40	10	180-545	97	-2	40.6 ± 0.6 (1.5%)
				40	2	180-545	96	-2	39.7 ± 0.4 (-0.8%)
	c)	**ET23-02**	Same specimen analyzed sequentially	40	25	180-535	97	1	41.5 ± 0.5 (3.8%)
				40	10	180-535	97	1	40.7 ± 0.3 (1.8%)
				40	2	180-535	97	-1	39.1 ± 0.2 (-2.3%)

Table S1